AIAA SciTech Forum
7-11 January 2019, San Diego, California
AIAA Scitech 2019 Forum

10.2514/6.2019-1591

Model Predictive Control Architectures for Maneuver Load Alleviation in Very Flexible Aircraft

Mateus de F. V. Pereira,* Ilya Kolmanovsky, † Carlos E. S. Cesnik, ‡
University of Michigan, Ann Arbor, Michigan, USA,

Fabio Vetrano§
Airbus Operations S.A.S., Toulouse, France

Two model predictive control (MPC) architectures to maneuver load alleviation in flexible and very flexible aircraft are considered. In the first, a tracking MPC formulation is used that directly manipulates the control inputs. In the second, MPC manipulates reference commands to the inner loop linear quadratic regulator (LQR) controllers. These MPC designs exploit full-order and reduced-order linearized models for prediction, and quadratic programming for computing the solutions. The performance of these control strategies is evaluated and compared through numerical simulations on nonlinear models of flexible and very flexible aircraft. Issues associated with the accuracy of the prediction model used in MPC design are discussed, particularly in view of the challenge of dealing with nonlinear very flexible aircraft dynamics.

I. Introduction

The current trends in aircraft design are towards higher-aspect ratio wings to enhance aerodynamic performance and decrease fuel consumption during flight [1]. At the same time, to implement such designs, weight constraints compel the use of lightweight materials and, inevitably, lead to more flexible structures and increasing challenges in dealing with loads induced by flight maneuvers, wind gusts and turbulence. One way to cope with larger loads and deflections is through the development of active maneuver load alleviation (MLA) systems.

The basic operating principles of the MLA system call for automatically deflecting the wing flight control surfaces, usually in a symmetric way, proportionally to the normal incremental acceleration of the airplane [2]. MLA systems can rely on wing deflection sensors, load factor sensors, or wing angle of attack sensors [2]. The basic idea in MLA is to concentrate lift inboard and reduce the wing bending moment at critical stations, which are usually located in the inner portion of the wing.

Depending on the level of structural flexibility, the aircraft can be classified either as flexible, such as current

*Graduate Research Assistant, Department of Aerospace Engineering.
†Professor, Department of Aerospace Engineering, AIAA Member.
‡Professor, Department of Aerospace Engineering, AIAA Fellow.
§Research and Development Engineer, Loads and Aeroelastics, Flight Physics.

airliners, or very flexible, such as high-altitude long-endurance (HALE) aircraft, which are considered for a multitude of future missions [3]. In the latter case, low frequency aeroelastic response may couple with flight dynamics modes, and nonlinearities can significantly affect the vehicle response. The design of such vehicles has brought significant challenges to aeronautical engineering since it requires geometrically nonlinear structural models for the primary structures in order to fully capture the large deformations that are likely to appear when the vehicle is subjected to operational loads [4]. From a control design standpoint, the large static and dynamic deformations in very flexible aircraft introduce state-dependent variations in the aircraft dynamics [5], and thus conventional control strategies are no longer suitable. MLA systems have a great potential to preserve the structural integrity of these vehicles.

In the existing literature, the design of the active control system for MLA has been approached using adaptive control [6–8], optimal control [9], model predictive control [10], fuzzy control [11], and other methods such as reference and extended command governors [12]. Similar design approaches were also considered for a related problem of gust load alleviation (GLA), see, e.g., [5, 13–16] and references therein. Due to the their ability to handle pointwise-in-time state and control constraints, the use of model predictive control (MPC) and reference governors (RG) aligns well with the main objective of MLA systems which is to ensure that loads do not exceed critical limits. In addition, these methods can be integrated with relative ease with other control design techniques, such as nonlinear, adaptive and robust control.

In this paper, two architectures for constrained control of flexible and very flexible aircraft are considered. In the first architecture, MPC is applied to the control inputs. In the second one, MPC modifies reference commands to two linear quadratic regulator (LQR) controllers if it becomes necessary to enforce the constraints. The objective is to demonstrate that these control approaches have a potential to satisfy MLA requirements on both flexible and very flexible aircraft, and assess how the level of flexibility affects the control design. To conduct such an assessment, modeling and numerical simulations were performed based on a nonlinear model representative of the University of Michigan's X-HALE unmanned aircraft.

The remaining sections of this paper are organized as follows. Section II revisits the conventional MLA control logic that has been implemented or proposed in the past along with control requirements. Sections III presents the theoretical formulation of the MPC solutions proposed. Section IV describes the equations of motion that are used to exemplify the two architectures for control design and for simulation of a flexible and very flexible aircraft. Section V presents simulation results based on nonlinear models. Finally, Section VI presents the conclusions from the numerical studies and comments on future research opportunities.

II. MLA System Requirements and Logic

The control requirements of an automatic flight control system with MLA capability are assumed as follows:

a) Track defined command signals and meet response specifications while ensuring stability during operation;

b) Keep loads at critical stations within pre-defined limits;

c) Minimize the effect of the MLA system on the nominal trajectory of the aircraft.

Traditional MLA approaches use accelerometers to measure the load factor and then deflect the control surfaces accordingly. In the system described in [17] for heavy transport civil aircraft, vertical accelerometers implanted at the front of the vehicle are used to detect and measure the vertical acceleration of the aircraft. If the vertical acceleration exceeds a predetermined threshold, the ailerons are activated and deflected by an angle proportional to the acceleration beyond the threshold. The definition of a threshold avoids repeated and superfluous operation of the control surfaces, which should be deflected only when the monitoring parameters at the selected stations are likely to reach a critical value.

The classical MLA logic based on acceleration is as follows [17]. Let $\ddot{z}(t)$ be the vertical acceleration at the instant t, where $t \in \{0, 1, 2, \ldots\}$ is the discrete time instant at which new acceleration measurements are available. The corresponding vertical load factor is given by:

$$n_z(t) = 1 + \frac{\ddot{z}(t)}{g}, \tag{1}$$

where g is the acceleration of gravity. Assume, for the purpose of this discussion, that $n_z(t) > 0$. Let n_z^s be a predetermined threshold (e.g., $2g$), and $n_z^{\max} > n_z^s$ denotes the maximum admissible vertical load factor (e.g., $2.5g$). Let $\delta u(t)$ be the deflection of the aileron, such that $\delta u(t) = \delta u_n(t) + k(t)\delta u_{\text{MLA}}$, where $\delta u_n(t)$ is the nominal deflection (e.g., the trim value or the deflection needed to perform a maneuver), δu_{MLA} is the maximum control surface deflection allowed for MLA purposes, and $0 \leq k(t) \leq 1$ is a gain. Define

$$\sigma(t) \triangleq \frac{n_z(t) - n_z^s}{n_z^{\max} - n_z^s}. \tag{2}$$

Then, the following cases apply:

1) If $n_z(t) \leq n_z^s$, then $k(t) = 0$;
2) If $n_z(t) > n_z^s$, and $n_z(t) \geq n_z(t-1)$, then $k(t) = \sigma(t)$;
3) If $n_z(t) > n_z^s$, and $n_z(t) < n_z(t-1)$, and $\sigma(t) \leq 0.1$, then $k(t) = \sigma(t)$;
4) If $n_z(t) > n_z^s$, and $n_z(t) < n_z(t-1)$, and $\sigma(t) > 0.1$, and $|\sigma(t) - k(t-1)| \leq 0.2$, then $k(t) = k(t-1)$;
5) If $n_z(t) > n_z^s$, and $n_z(t) < n_z(t-1)$, and $\sigma(t) > 0.1$, and $|\sigma(t) - k(t-1)| > 0.2$, then $k(t) = \sigma(t)$.

In cases 3 and 4 the tendency of load factor to decrease is confirmed and a hysteresis is implemented, so as to not adversely affect the stability of the aircraft. The MLA system is only activated when one of cases 2-5 is true and the aircraft is in flight, in a cruise configuration (leading edges and wing flaps retracted), and the control stick is deflected beyond a certain angular threshold for confirming the maneuver (e.g. 8 deg in a nose-up direction). The advantage of using the load factor for MLA relies on the fact that acceleration measurements are easily obtained and sensors have a

high degree of reliability.

Other MLA systems rely on measurements of loads at critical stations on the wing and horizontal tail (e.g. bending moment at the wing/horizontal stabilizer root) and pursue the objective of keeping the loads at these stations within the specified safety limits. These are set based on structural properties and design, while ensuring minimum impact on the performance and trajectory of the aircraft. Approaches along these lines for MLA and GLA include [6, 16, 18–21]. The direct treatment of loads rather than the use of load factor is advantageous since the ultimate goal is to restrain the maximum load exerted on the structure during flight.

Loads, such as the wing root bending moment, can be inferred from strain gauge sensor measurements. Considering the wing modeled as an Euler-Bernoulli beam, the axial strain at some point at spanwise station y and z distance from its neutral surface is given by

$$\epsilon_{yy} = -\kappa_x z, \tag{3}$$

where κ_x is the curvature about the x axis. The resultant bending moment M_x is giving by:

$$M_x = EI_{xx}\kappa_x, \tag{4}$$

where EI_{xx} is the out-of-plane bending stiffness at wing station y. Note that a similar logic for the MLA system described previously can be used with bending moment in lieu of load factor.

Consequently, in the subsequent designs being considered, constraints are imposed on the out-of-plane curvature κ_x at the wing root so as to limit the bending moment at this station. The MPC and reference governors can directly enforce such constraint. Note that this allows to operate the aircraft at the extreme of the design envelope so that to obtain the best performance without violating the safety limits. In this sense, the controller will only actively perform load alleviation (i.e., deflect the control surfaces to reduce the variation of the curvature) when κ_x is close to the upper or lower bounds. Otherwise, the MLA controller will not engage so that to preserve the trajectory commanded to the aircraft.

Note that no minimum load threshold specification is necessary to trigger the MLA system when the MPC is used. This is replaced by the prediction step in MPC, which foresees imminent constraint violations within a pre-defined prediction horizon. As a result, the MLA system prevents the violation of the load constraints rather than reacting to them, as it happens in the traditional MLA systems. Other output and input constraints can also be handled by the MPC based controller in addition to the curvature constraints used for MLA. Hence, when compared with the aforementioned traditional MLA system, the new MPC design is more versatile and potentially less conservative. It is able to handle multiple constraints at different stations on the vehicle, actively preventing critical loads exceeding the safety limits while meeting the control requirements a) - c) discussed at the beginning of this Section, and safely exploiting the entire

flight envelope.

III. Model Predictive Control for MLA

The considered objective for the development of the MLA control solution is performing a prescribed maneuver by tracking command signals while enforcing input and output constraints (Sec. II).

The prediction model for the aircraft dynamics is derived starting from a continuous-time linearized model around a defined flight condition, i.e.,

$$\begin{bmatrix} \dot{x}_F \\ \dot{x}_R \end{bmatrix} = \begin{bmatrix} A_{FF} & A_{FR} \\ A_{RF} & A_{RR} \end{bmatrix} \begin{bmatrix} x_F \\ x_R \end{bmatrix} + \begin{bmatrix} B_F \\ B_R \end{bmatrix} u = Ax + Bu, \tag{5}$$

$$y = Cx + Du, \tag{6}$$

where $x = [x_F^T \;\; x_R^T]^T \in \mathbb{R}^{n_x}$ is the state vector, $u \in \mathbb{R}^{n_u}$ is the input vector, $y \in \mathbb{R}^{n_y}$ is the output vector, and subscripts F and R stand for flexible and rigid, respectively. For design purposes, the input vector is divided into control effectors u_a that manipulate the aircraft attitude, effectors u_T that manipulate the total thrust, and effectors u_{MLA} used to perform MLA:

$$u = \begin{bmatrix} u_a^T & u_T^T & u_{\text{MLA}}^T \end{bmatrix}^T. \tag{7}$$

A subset of the outputs, $y^{\text{t}} = C^{\text{t}}x$, $C^{\text{t}} \in \mathbb{R}^{n_r \times n_x}$, $n_r \leq n_y$, is to be controlled to set-points. The vector of set-points is denoted by $r \in \mathbb{R}^{n_r}$. In this work, the components of r are target values (in terms of deviations from the trim values) for aircraft longitudinal velocity, heading angle, flight path angle and side-slip angle, i.e.,

$$r = \begin{bmatrix} r_V & r_\psi & r_\gamma & r_{\beta_s} \end{bmatrix}^T. \tag{8}$$

The tracking error is defined as

$$e = y^{\text{t}} - r. \tag{9}$$

Two control architectures that use MPC are introduced in this paper. In the first (Fig. 1a), referred here as the MPC architecture, a tracking MPC formulation is used that directly manipulates the control effectors. In the second (Fig. 1b), referred here as the RG architecture, MPC manipulates reference commands to existing inner loop controller, which in this work is assumed to be designed based on two linear quadratic regulator (LQR) controllers with integral action (LQ-I).

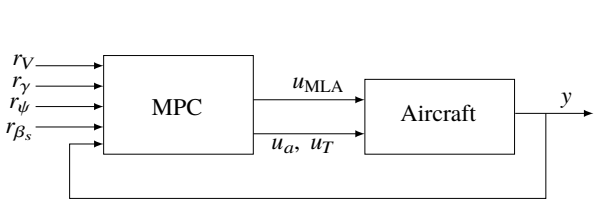

(a) MPC Architecture: MPC as an integrated flight control system

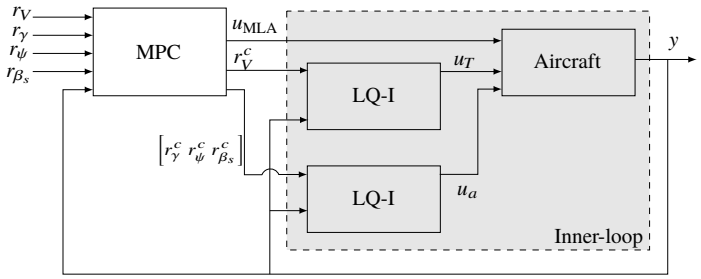

(b) RG Architecture: MPC as a reference governor

Figure 1 MPC architectures for MLA.

A. MPC Architecture

The MPC architecture in Fig. 1a is conceived as an integrated flight control system [14], that is, it is responsible for both command tracking and load alleviation. In this sense, the controller not only prevents the aircraft from exceeding structural safety limits, but also makes use of the aircraft flexibility to potentially improve the aircraft performance by computing the optimal control action based on predictions of both rigid and flexible dynamics.

For the MPC design, the linear model in Eqs. 5 and 6 is converted to discrete-time assuming a zero-order hold with the sampling time T_s so that the control inputs are constant over each sampling period. The discrete-time linear prediction model has the following form:

$$\begin{aligned} x_{k+1} &= A_d x_k + B_d u_k, \\ y_k &= C_d x_k + D_d u_k, \qquad (10) \\ y_k^{\text{t}} &= C_d^{\text{t}} x_k, \qquad (11) \end{aligned}$$

where $A_d \in \mathbb{R}^{n_x \times n_x}$, $B_d \in \mathbb{R}^{n_x \times n_u}$, $C_d \in \mathbb{R}^{n_y \times n_x}$, $D_d \in \mathbb{R}^{n_y \times n_u}$.

To design a tracking MPC controller, the following augmented vector is defined:

$$x_k^{\text{aug}} \triangleq \begin{bmatrix} \Delta x_k^T & x_k^T & u_k^T \end{bmatrix}^T \in \mathbb{R}^{2n_x+n_u}, \qquad (12)$$

where $\Delta x_k = x_{k+1} - x_k$. This is the so-called incremental rate-based MPC formulation, which results in a robust augmentation of the controller with an integral action. This ensures (under reasonable assumptions) zero steady-state tracking error even when a mismatch between the model used for the design and the actual plant is present.

The MPC feedback law is defined by the first element of the control sequence that is solution to the following

constrained discrete-time optimal control problem:

$$\underset{\Delta u_0, \Delta u_1, \ldots, \Delta u_{N-1}, \varepsilon}{\text{minimize}} \; J_N = ||e_N||_P^2 + \sum_{k=0}^{N-1} ||e_k||_Q^2 + ||\Delta u_k||_R^2 + ||(u_{\text{MLA}})_k||_{R_{\text{MLA}}}^2 + \mu\varepsilon^2, \tag{13}$$

subject to:

$$\begin{aligned} x_{k+1}^{\text{aug}} &= A^{\text{aug}} x_k^{\text{aug}} + B^{\text{aug}} \Delta u_k, \\ e_{k+1} &= \begin{bmatrix} C_d^t & 0 & 0 \end{bmatrix} x_k^{\text{aug}} + e_k, \\ x_0^{\text{aug}} &= \text{current state}, \\ p(x_k^{\text{aug}}) &\leq \varepsilon, \\ g(\Delta u_k) &\leq 0, \; k = 0, \cdots, N-1, \\ \varepsilon &\geq 0, \end{aligned} \tag{14}$$

where $\Delta u_k = u_{k+1} - u_k$, $e_k = y_k^{\text{t}} - r$, N is the prediction horizon, Q, R, R_{MLA} and P are symmetric positive definite weighting matrices, and $\mu > 0$ is a scalar weight. The term containing P in Eq. 13 is a terminal penalty that is used to enhance the stability characteristics of the closed-loop system, specifically to guarantee local stability if constraints are inactive. This cost function given by Eq. 13 is minimized with respect to $\{\{\Delta u_k\}_{k=0}^{N-1}, \varepsilon\}$ and subject to the imposed state, output and control constraints.

The functions $p(\cdot)$ and $g(\cdot)$ in Eq. 14 represent the state and control constraints, respectively, while ε is a slack variable used to relax the constraints on states and outputs if necessary so that it is always possible to guarantee feasibility of the optimization problem. As feasibility is trivially enforced on input constraints, they are treated as hard constraints.

To ensure local stability, the terminal penalty is usually computed as the solution of the algebraic Riccati equation for the corresponding discrete time system model. However, the augmented system in Eq. 14 may not be controllable due to the augmentation of the states x_k and u_k to the state vector, which implies that a stabilizing solution cannot be found. To work around this issue, the terminal penalty is computed on Δx_N and e_N only, defined based on the solution of the algebraic Riccati equation for the subsystem which represents the dynamics of Δx_k and e_k.

The cost function in Eq. 13 includes a penalty on u_{MLA} in addition to the usual penalization of its rate of change Δu_{MLA}. The penalty on u_{MLA} ensures that the control effectors used for MLA, usually ailerons and/or elevators, return back to the trim condition after performing load alleviation. This is desired to minimize drag and deviation from the nominal trajectory when the MLA system is deactivated. Note that the control efectors assigned to perform MLA are not dedicated, meaning that, in addition to performing MLA, they can also assist the effectors u_a and u_T for attitude and thrust control. This supplementary behavior can be minimized by tuning the controller, usually by choosing the weights

on u_{MLA} greater than the weights on the remaining control effectors.

B. RG Architecture

In the RG architecture shown in Fig. 1b, the MPC controller plays the role of a reference governor for the inner loop, in addition to manipulating the extra degrees of freedom provided by u_{MLA} to perform MLA. The signal tracking task is assigned to the inner loop. Appealing features of this architecture include the preservation of the nominal controller in the inner loop, which can be advantageous from a design perspective, since the conventional flight control system is augmented rather than replaced. Moreover, the performance and stability of the vehicle is protected even if the outer loop has to be deactivated.

In this work, as an illustration, the reference governor augmentation of a nominal LQ-I type controller is considered. Such a controller is frequently used in aerospace applications due to the ease of design and implementation. Here, such an LQ-I controller can track the set-points r by manipulating the control effectors u_a and u_T. To design this inner loop controller, the rigid body part of the linear continuous-time model in Eq. 5 is used. Note that u_{MLA} is assumed to be zero, as the controller only manipulates u_a and u_T control inputs, aggregated into the control vector $u_{il} = [u_a^T \quad u_T^T]^T$. To obtain the residualized linear model for the rigid-body dynamics with states $x_R \in \mathbb{R}^{12}$, the flexible states are assumed to be in steady-state, yielding:

$$\dot{x}_R = \left(A_{RR} - A_{RF}A_{FF}^{-1}A_{FR}\right)x_R + \left(B_R - A_{RF}A_{FF}^{-1}B_F\right)u_{il} = \bar{A}_R x_R + \bar{B}_R u_{il}. \tag{15}$$

The LQ-I control design for u_{il} can be based on minimizing the following cost function,

$$J = \int_0^\infty (e(t)^T Q_e e(t) + \dot{u}_{il}^T(t) R \dot{u}_{il}(t))dt, \tag{16}$$

where Q_e and R are positive definite weighting matrices and $e(t)$ is the tracking error of the inner loop. The control input obtained from the solution of this optimal control problem has the form:

$$u_{il}(t) = u_{il}(0) + K_1(x_R(t) - x_R(0)) + K_2 \int_0^t (y^{\text{t}}(t) - r)dt, \tag{17}$$

where K_1 and K_2 are constant gains. Equation (17) shows that the control law has an integral action, which is the feature that allows the tracking of commands with zero steady-state offset.

For the aircraft models considered in this work (see Section IV), it was deemed advantageous to implement two separate LQ-I controllers which independently manipulate u_a and u_T control channels. In particular, these two LQ-I loops appear to require gains of different magnitude; hence a single LQ-I controller is not straightforward to tune to obtain desirable stability and good performance characteristics, and this task is simplified with two separate LQ-I

controllers. The design of these two separate LQ-I controllers is based on Eqs. (15)-(17) adopted to each of the two input-output combinations consistently with Fig. 1b.

Note that the LQ-I controller design has a closed form solution, which is straightforward to implement since no real-time optimization is involved. On the other hand, the LQ-I design alone has no means of enforcing state and control constraints. An MPC controller to govern the references while enforcing constraints is then considered. This approach is closest to the extended command governor in [22–24] but novel and different in terms of details and implementation. The MPC controller computes the references $r^c = [r_V^c \;\; r_\psi^c \;\; r_\gamma^c \;\; r_{\beta_s}^c]^T$ to be fed into the inner loop in order to prevent constraint violations. In addition, the MPC controller computes the control action for u_{MLA} to perform MLA when a violation of the curvature constraint is imminent. In the event the constraints are inactive, $r^c \rightarrow r$ and u_{MLA} returns to the trim condition.

To design the MPC controller to work as a reference governor, a discrete-time linear system model representative of the inner loop system consisting of LQ-I controllers and the plant is derived. Note that now both the flexible and rigid dynamics of the plant are considered. To include the control effectors u_{MLA} as control inputs, columns are added to the control matrix of the inner loop system so that the discrete-time model becomes:

$$x_{k+1} = A_r x_k + \begin{bmatrix} B_r & 0 \\ 0 & B_{\text{MLA}} \end{bmatrix} \begin{bmatrix} r_k^c \\ u_{\text{MLA}} \end{bmatrix} = A_r x_k + \bar{B}_r u_k^r, \tag{18}$$

where B_{MLA} are the columns of B in Eq. 5 corresponding to u_{MLA}. Note that since the reference governor is applied to the inner loop system, control constraints can be reformulated as equivalent constraints on the states of the plant, states of the inner loop controller, and references.

The optimization problem is defined to achieve tracking of r by r_k^c subject to constraints and is stated as follows:

$$\underset{\Delta u_0^r, \Delta u_1^r, \ldots, \Delta u_{N-1}^r, \varepsilon}{\text{minimize}} \; J_N = \sum_{k=0}^{N-1} ||r_k^c - r||_{Q_r}^2 + ||\Delta u_k^r||_{R_r}^2 + ||(u_{\text{MLA}})_k||_{R_{\text{MLA}}}^2 + \mu\varepsilon^2, \tag{19}$$

subject to:

$$\begin{aligned} x_{k+1}^{\text{aug}} &= A_r^{\text{aug}} x_k^{\text{aug}} + B_r^{\text{aug}} \Delta u_k^r, \\ x_0^{\text{aug}} &= \text{current state}, \\ h(x_k^{\text{aug}}) &\leq \varepsilon, \\ m(u_{\text{MLA}}) &\leq 0, \\ \varepsilon &\geq 0, \end{aligned} \tag{20}$$

where $x_k^{\text{aug}} = [x_k^T \quad u_k^T]^T$ is an augmented vector, $\Delta u_k^r = u_{k+1}^r - u_k^r$, $h(\cdot)$ represents inequality constraints on the states and outputs of the augmented system, and $m(u_{\text{MLA}})$ are the constraints on the control effectors used for MLA. The inclusion of the penalty on u_{MLA} in the cost function in Eq. 19 is motivated by the same reasons discussed in Section III.A.

IV. Aircraft Models

To illustrate the MPC solutions presented in Section III, nonlinear models for a flexible aircraft and very flexible aircraft are derived from the X-HALE aircraft.

A. X-HALE

The X-HALE is a very flexible, remote-piloted aircraft developed at the University of Michigan with the primary objective to collect experimental aeroelastic data and to serve as a platform to evaluate control strategies [3]. It was modeled using the University of Michigan's Nonlinear Aeroelastic Simulation Toolbox (UM/NAST) [25], that employs geometrically nonlinear strain based finite elements, different options for steady and unsteady aerodynamics, and nonlinear 6-degree of freedom (DOF) rigid body equations of motion to numerically simulate the dynamics of the aircraft.

The X-HALE aircraft is shown in Fig. 2. It is a wing-boom-tail type aircraft with a 6-meter span, divided into six sections of 1-meter long each, with the tip sections set at a dihedral angle of 10 deg. The wing has an EMX-07 airfoil profile with 0.2 m chord, while the tails employ the NACA 0012 airfoil profile with chord length of 0.12 m [3].

Figure 2 The University of Michigan's X-HALE aircraft.

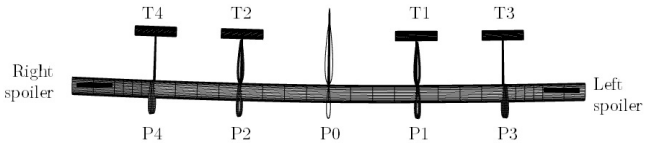

Figure 3 Control effectors on X-HALE; elevators T3 and T4 are the primary control surface used for load alleviation.

As shown in Fig. 3, there are eleven control effectors available: two roll spoilers located at the dihedral sections, four elevators situated at each outboard tail (represented by T1-T4), and five motors (represented by P0-P4). The center tail is not used as a control surface. For control design, six control inputs are considered, namely, the inner elevator deflection $\delta_{T1,T2}$ (symmetrical for both surfaces), the outer elevator deflection on the right wing δ_{T4}, the outer elevator deflection on the left wing δ_{T3}, the roll spoiler deflection δ_{sp} (given by the difference between the deflection of the right and left spoilers), the differential thrust δ_{dT} (difference between the revolutions per second of the left motors and right motors), and the overall thrust δ_T (average of revolutions per second of all motors). Note that the spoiler can only have positive deflection.

The spoilers, differential thrust, and inner elevators are the main inputs used to control the attitude of the aircraft. The outer elevators, working independently, are the primary surfaces used to control the geometry of the wing to avoid any violation of the safety limits. These two control surfaces have more control authority over the geometry when compared to the inner elevators since they are placed further outboard and, therefore, can produce a higher moment. The ability to deflect up and down, thus producing positive and negative moments on the main wing, gives a significant advantage over the spoilers. Note that, when not being used for MLA, the outer elevators can still be used for pitch control if necessary. To be consistent with the notation introduced in Section III, the following input vectors are defined:

$$u_{\text{MLA}} = \begin{bmatrix} \delta_{T3} & \delta_{T4} \end{bmatrix}^T, \qquad u_a = \begin{bmatrix} \delta_{T1,T2} & \delta_{sp} & \delta_{dT} \end{bmatrix}^T, \qquad u_T = \delta_T. \tag{21}$$

In order to represent the response of flexible aircraft, the X-HALE model in UM/NAST has been modified by increasing the stiffness matrix of the original X-HALE model by a factor of two. Figure 5 shows the trim shape of the two models at 14 m/s. For this flight speed, the wing tip deflection was reduced from 10.52% to 5.25%.

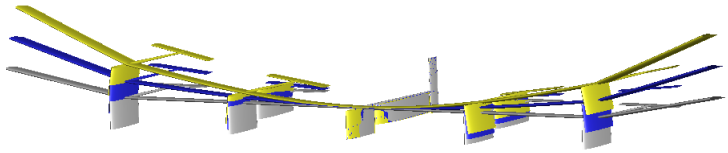

Figure 4 Difference in X-HALE trimmed shape at 14 m/s for the original, very flexible model (yellow), the stiffened model (blue), and the reference undeformed configuration (gray)

B. Nonlinear Equations of Motion

From [25], each beam element has four degrees of freedom: extensional (ϵ_{yy}), twist (κ_y) and two orthogonal bending curvatures of the beam reference line, representing the out-of-plane (κ_x) and in-plane bending (κ_z). The strain vector for the ith element is given by

$$\epsilon_i = \begin{bmatrix} \epsilon_{yy,i} & \kappa_{x,i} & \kappa_{y,i} & \kappa_{z,i} \end{bmatrix}^T. \tag{22}$$

Let b be a vector that aggregates the position (p_B) and orientation (Θ_B) components of the body-fixed frame relative to an inertial frame resolved in the body-fixed frame:

$$b = \begin{bmatrix} p_B^T & \Theta_B^T \end{bmatrix}^T. \tag{23}$$

The rigid body motion of the body fixed frame is described by the three linear velocities ($V_B = [u_B \;\; v_B \;\; w_B]^T$) and

three angular rates (ω_B) expressed in the body fixed frame as:

$$\beta = \begin{bmatrix} V_B^T & \omega_B^T \end{bmatrix}^T. \tag{24}$$

Note that $\dot{b} \neq \beta$ unless Θ_B is small. The attitude and inertial displacement of the body fixed frame are represented by quaternions and the displacement vector, respectively, as:

$$\zeta = \begin{bmatrix} q_0 & q_1 & q_2 & q_3 \end{bmatrix}^T, \tag{25}$$

$$P_B = \begin{bmatrix} x_B & y_B & z_B \end{bmatrix}^T. \tag{26}$$

The coupled nonlinear aeroelastic and rigid body equations of motion have the following general form:

$$M(q)\ddot{q} + C(q,\dot{q})\dot{q} + Kq = R(q,\dot{q},\zeta,u_c), \tag{27}$$

and the frame propagation equations:

$$\dot{\zeta} = -\frac{1}{2}\Omega(\beta)\zeta, \tag{28}$$

$$\dot{P}_B = \begin{bmatrix} C^{GB} & 0_{3\times 3} \end{bmatrix}\beta, \tag{29}$$

where $q = \begin{bmatrix} \epsilon^T & b^T \end{bmatrix}^T$, $u_c = \begin{bmatrix} u_a^T & u_T^T & u_{\text{MLA}}^T \end{bmatrix}^T$ is the control input, $M(q)$ is the generalized mass matrix, $C(q,\dot{q})$ is the generalized damping matrix, K is the generalized stiffness matrix, $R(q,\dot{q},\zeta,u_c)$ is the state-dependent generalized force vector, $\Omega(\beta)$ is the matrix for propagating the first-order quaternion differential equations, and C^{GB} is the transformation matrix from the body-fixed frame to the inertial frame, which is represented in terms of quaternions. The vector ϵ concatenates the strain vector for the n elements in the structure, that is, $\epsilon = [\epsilon_1^T\ \epsilon_2^T \cdots \epsilon_n^T]^T$.

Equations (27) to (29) are used to reproduce the dynamics of the aircraft in both open and closed-loop nonlinear simulations in UM/NAST. However, for control design purposes, Euler angles $[\phi\ \theta\ \psi]^T$ are chosen in lieu of quaternions. The attitude of the body frame with respect to the inertial frame in Euler angle representation can be recovered from quaternions as [26]:

$$\begin{aligned} \phi &= = \tan^{-1}\left(\frac{2q_2q_3 + 2q_0q_1}{q_0^2 - q_1^2 - q_2^2 + q_3^2}\right), \\ \theta &= -\sin^{-1}\left(2q_1q_3 - 2q_0q_2\right), \\ \psi &= \tan^{-1}\left(\frac{2q_1q_2 + 2q_0q_3}{q_0^2 + q_1^2 - q_2^2 - q_3^2}\right). \end{aligned} \tag{30}$$

The angle of attack, side-slip and flight path angles, which are parameters related to the flight performance of the aircraft, can also be obtained as:

$$\text{Angle of attack} \quad \alpha = \tan^{-1}\left(\frac{w_B}{u_B}\right), \tag{31}$$

$$\text{Side-slip angle} \quad \beta_s = \sin^{-1}\left(\frac{v_B}{||V_B||}\right), \tag{32}$$

$$\text{Flight path angle} \quad \gamma = \sin^{-1}\left(\frac{\dot{z}_G}{||V_B||}\right), \tag{33}$$

where $||V_B|| = V = \sqrt{u_B^2 + v_B^2 + w_B^2}$, $\dot{z}_G$ is the vertical velocity of the vehicle in the inertial frame, and u_B, v_B and z_B are the components of velocity resolved in the body-fixed frame.

C. Linear Models for Control Design

The control architectures studied in this work are based on linear models. Therefore, the nonlinear dynamics are linearized around the trim condition to obtain equations of the form shown in Eqs. 5-6, where x is the state vector that represents the deviation of $\begin{bmatrix} \epsilon^T & \dot{\epsilon}^T & \beta^T & \zeta^T & P_B^T \end{bmatrix}^T$ from the trim values, u is the control input vector that represents the deviation of u_c from the trim values, and y is the output vector that represents the deviation of

$$\begin{bmatrix} \kappa_{x_{right}} & \kappa_{x_{left}} & \beta^T & \zeta^T & P_B^T & \alpha & \beta_s & \gamma & V_B \end{bmatrix}^T,$$

from trim values, where $\kappa_{x_{right}}$, $\kappa_{x_{left}}$ denote the out-of-plane curvatures at the wing root of the right wing and the left wing, respectively. In this study, the matrices A, B, C and D were obtained for a trim configuration at 14 m/s forward speed and altitude of 30 m for both flexible and very flexible models. The full-order linear model has a total of 60 states, 6 control inputs and 17 outputs. Note that the flexible states ϵ and $\dot{\epsilon}$ are usually not available for feedback, and therefore an observer has to be integrated into the control system for real time estimation of these signals. This work considers full state feedback, and leaves the treatment of the observer to future work.

While for flexible aircraft the structural deformations are relatively small and the nonlinear dynamics can be well approximated by a linear model around the trim condition, for very flexible aircraft may no longer be the case as one has to account for geometric nonlinearities of the flexible structure. In general, these nonlinear effects start to be significant when the wing tip deflections with respect to the undeformed geometry, and normalized with respect to the semi-span, exceed 10%. A degradation of the control performance may occur in this situation.

In addition, by decreasing the stiffness of the vehicle, the controllability of the linearized model decreases, as shown in Fig. 5. In particular, the minimum singular value $\sigma_{\min}(W_c)$ of the controllabity grammian W_c is lower for very flexible aircraft. From a theoretical point of view [27], this means that the control cost to bring the aircraft states to trim

values increases in the very flexible aircraft case versus the flexible aircraft case.

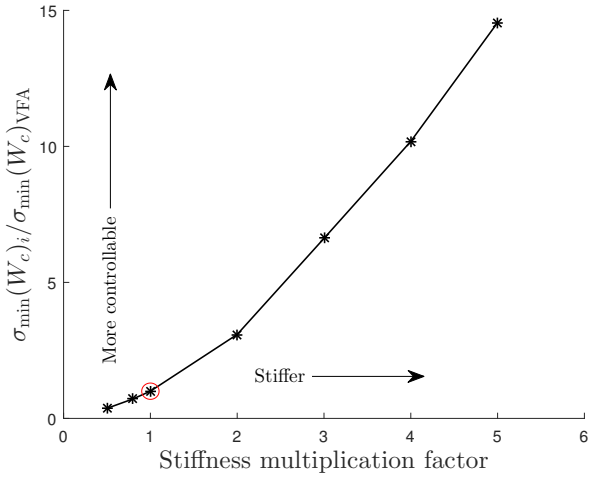

Figure 5 Minimum singular value of the controllability grammian, normalized with respect to the value for the original X-HALE (shown by ○) and denoted by $\sigma_{\min}(W_c)_{\mathrm{VFA}}$, as a function of stiffness.

In order to lower the computational cost of the control design, reduced-order models (ROM) may be used. When performing model order reduction one seeks to represent a system by a lower dimensional model that can still capture the dominant characteristics of the system response. Towards this end, balanced truncation is used here [28].

V. Simulation Results

In this section, the results of the numerical simulations of the two control architectures proposed in Sections III are presented. The linearized full-order model and ROMs of the flexible and very flexible aircraft discussed in Section IV are used for control design. To obtain the ROMs, the augmented models used in the MPC optimization, Eqs. 14 and 20, were reduced from 128 states to 70 states. The closed-loop simulations were performed using the nonlinear models for both aircraft in the UM/NAST environment.

In the simulations, the aircraft flies in closed-loop configuration at the trim condition for 1.0 s and then a pitch up maneuver is commanded. The objective is to reach the flight path angle of $r_\gamma = 8$ deg while maintaining the same speed, and keeping the heading and side-slip angles close to zero.

The constraints imposed on the control problem are shown in Table 1. Note that the constraints on the out-of-plane curvature at the wing root are defined according to the MLA objective discussed in Section II, and their limits are chosen according to the variation allowed with respect to the trim condition. In addition to these constraints, limits on the control effector values and rates are imposed, and limits on the angle of attack to prevent stall.

Since all constraints considered in this application are box constraints, the optimization problems defined in Section III.A and III.B are convex and can be solved by conventional quadratic programming solvers. In this work, qpOASES

Table 1 Output and input constraints.

Variable	Description	Min	Max	Unit
$\kappa_{x_{right}}$, $\kappa_{x_{left}}$ (flexible)	Out-of-plane curvature at wing root on flexible aircraft model	0.041	0.063	[1/m]
$\kappa_{x_{right}}$, $\kappa_{x_{left}}$ (very flexible)	Out-of-plane curvature at wing root on very flexible aircraft model	0.096	0.110	[1/m]
α	Angle of attack	-10	10	[deg]
$\delta_{T1}, \delta_{T2}, \delta_{T3}, \delta_{T4}$	Elevator deflection	-30	30	[deg]
δ_{sp}	Spoiler deflection	0	30	[deg]
δ_{dT}	Differential thrust	50	-50	[rps]
δ_T	Average propeller rotation	20	120	[rps]
$\Delta\delta_{T1}, \Delta\delta_{T2}, \Delta\delta_{T3}, \Delta\delta_{T4}, \Delta\delta_{sp}$	Rate of deflection of elevators and spoilers	-90	90	[deg/s]
$\Delta\delta_{dT}, \Delta\delta_T$	Rate of variation of propeller rotation	-50	50	[rps/s]

[29] was used, which is an open source C++ code based on an online active set optimization algorithm.

For both controllers, the sampling rate is 50 Hz and the prediction horizon is 100 steps. This means that the MPC controllers looks 2 s ahead of the current time to predict constraint violations and then determine the optimal control action.

A. Flexible Aircraft

Figure 6 shows the time histories of the out-of-plane curvature and corresponding bending moment at the right and left wing root, and the wing tip deflection as a percentage of its semi-span. For all of this, the stiffened X-HALE is performing the prescribed maneuver with the MPC architecture (Fig. 6a) and the RG architecture (Fig. 6b). In red, the results for the the case when no constraints on the curvature are imposed (i.e., no MLA is performed) are shown, and the full-order linear model is used for prediction. In black, the results for the case in which the curvature constraints are activated and the prediction is also based on the full-order model are shown. The blue curve is similar to the latter case, but the prediction is based on the ROM. In the simulation with the MPC architecture, the curvature constraint was satisfied, which resulted in an alleviation of approximately 46.3% at each semi-wing, when either the full-order model or ROM were used. In the results for the RG architecture, there was a slight violation of the constraint when the ROM was used. As a result, the load alleviation was around 40.2% for the full-order model, and approximately 32.7% for the case with the ROM. It is worth noting that for both simulations, the wing tip deflection remained below 10%, which indicates that nonlinear effects, even though present, were not strong.

Figure 7 shows the tracking variables. For all controllers, the tracking targets were reached within reasonable time, and with similar performance when either full-order model or ROM was used for prediction.

The control inputs computed by the controllers in the MPC architecture and the RG architecture are shown in Fig. 8a and Fig. 8b, respectively. To perform the pitch up maneuver, the inner elevators δ_{T1} and δ_{T2} were the primary control

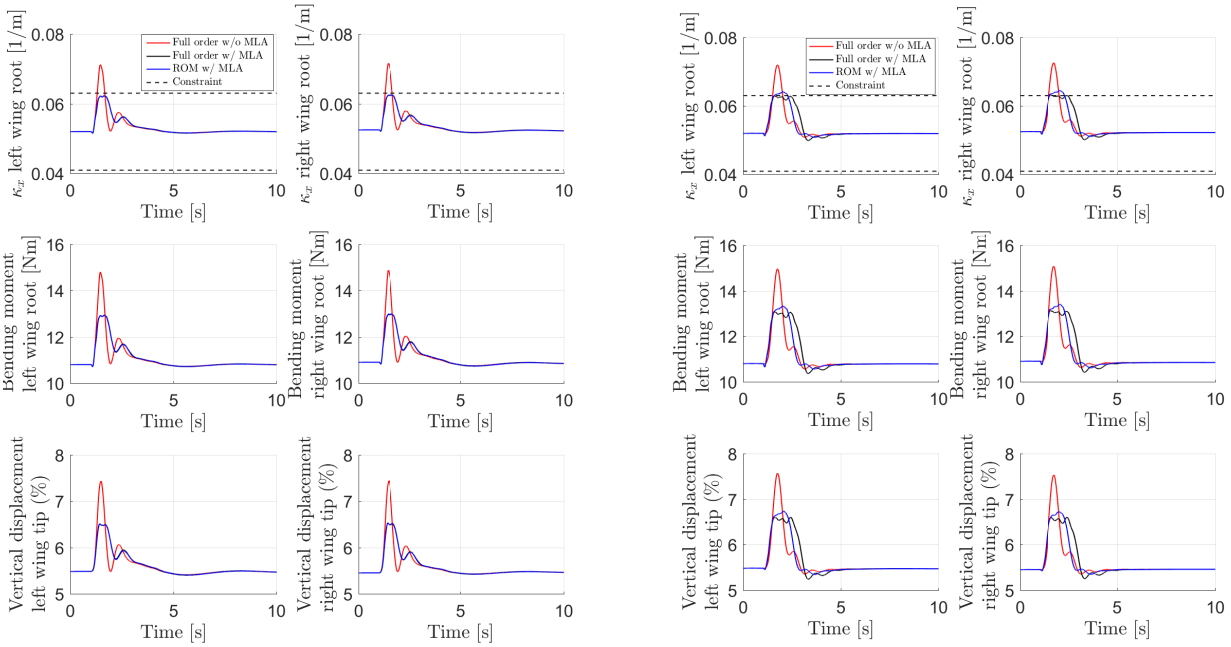

(a) MPC architecture. **(b) RG architecture.**

Figure 6 X-HALE flexible model closed-loop simulations for load alleviation using two different control architectures.

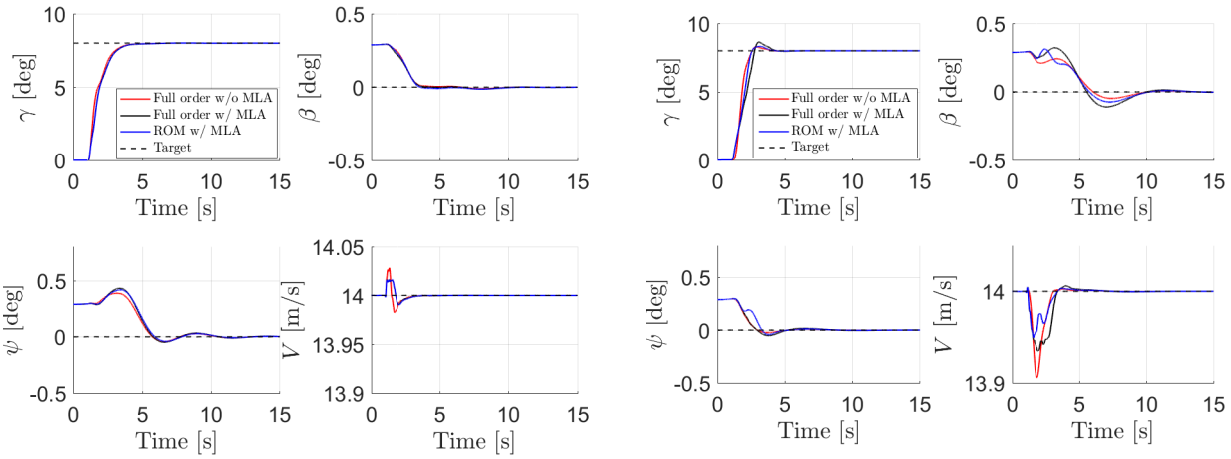

(a) MPC architecture. **(b) RG architecture.**

Figure 7 Command tracking performance of the X-HALE flexible aircraft.

effectors used, while the spoilers and differential thrust were used to control the lateral motion of the vehicle. Note that the outer elevators δ_{T3} and δ_{T4} remained at the trim condition when the MLA system was deactivated. After performing the load alleviation, these elevators returned to their initial position. In the simulations with the MPC architecture, the outer elevators interestingly behaved in a different manner than in the other architecture. To perform MLA, the MPC

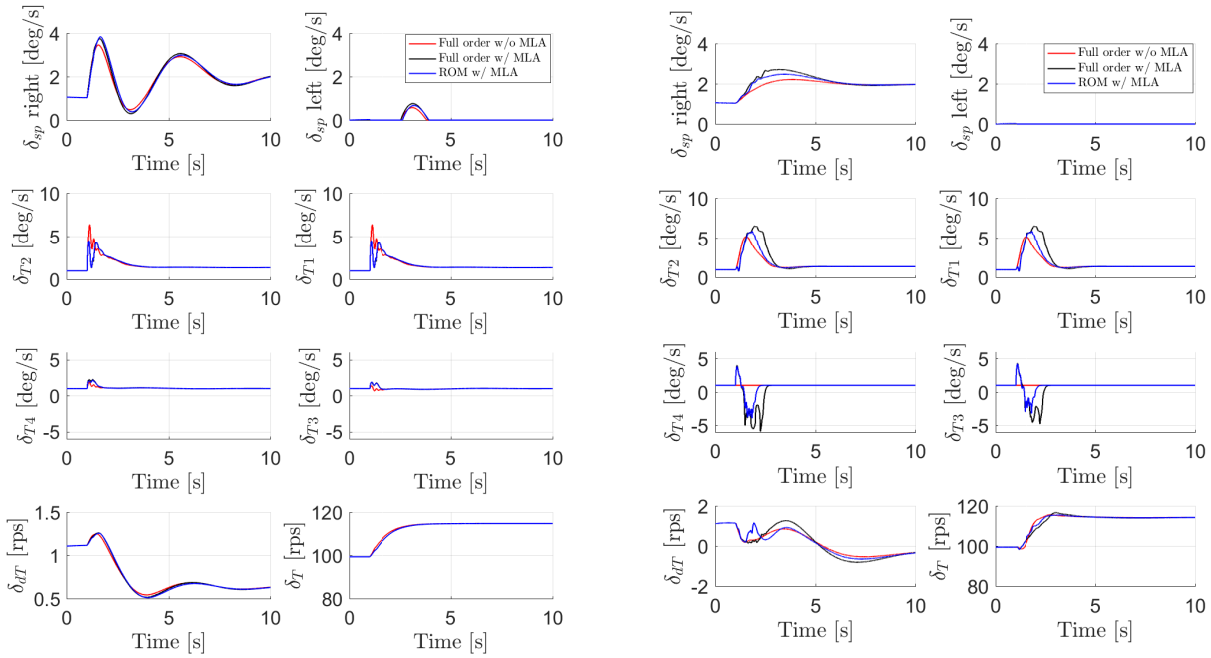

(a) MPC architecture. **(b) RG architecture.**

Figure 8 Time histories of control inputs of X-HALE flexible aircraft.

controller found the optimal solution to be the redistribution of the control effort to pitch up the vehicle among the four elevators by deflecting all of them upwards.

The actuation of the outer elevator to perform MLA had little impact on the nominal trajectory of the airplane. As shown in Fig. 9, the deviation with respect to the nominal case, computed as a percentage of the difference between the Euclidian norm of the position of the aircraft in each simulation, is below 0.4%.

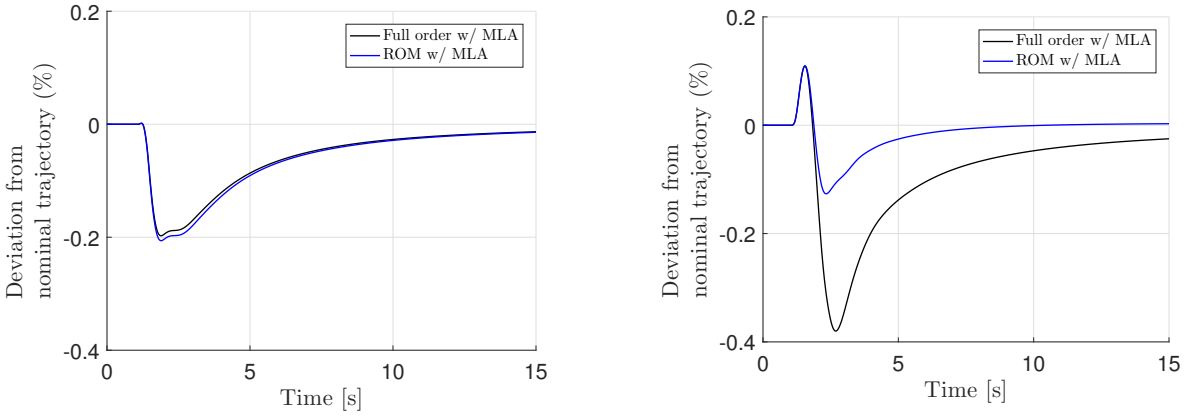

(a) MPC architecture. **(b) RG architecture.**

Figure 9 Trajectory deviation of the X-HALE flexible aircraft.

B. Very Flexible Aircraft

Figure 10 shows the out-of-plane curvature and the corresponding bending moments at the right and left wing root, and the wing tip deflection for the very flexible X-HALE aircraft model performing the pitch up maneuver with both control architectures. There was no constraint violation. However, the ROM in the RG architecture overestimated the wing curvature, resulting in a greater load alleviation than expected. While the load alleviation with the full-order model was around 42.7%, it reached 56.5% for the case with the ROM. When the MPC architecture was used, the load alleviation with either linear model was approximately 50.7% at each semi-wing. The wing tip deflection was above 10% in all cases tested, which indicates that the nonlinear effects may not be insignificant, and consequently the prediction obtained with the linear ROM model may be degraded.

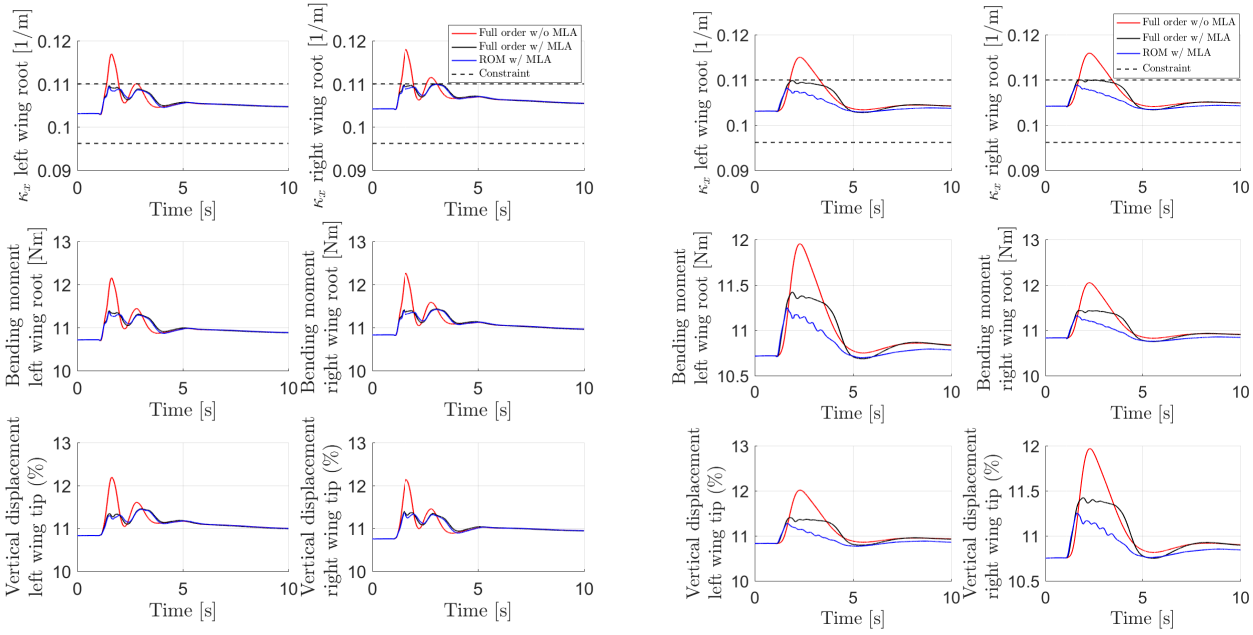

(a) MPC architecture.

(b) RG architecture.

Figure 10 X-HALE very flexible model closed-loop simulations for load alleviation using two different control architectures.

Similar to the results in Section V.A for the flexible aircraft, both control architectures were successful in tracking the commanded references. Note, however, that the flight path angle rise is slower for this aircraft. Due to the nonlinear characteristics of the very flexible aircraft dynamics, high accelerations can cause significant deformations of the structure during the maneuver. As a matter of fact, both architectures perform poorly in such situations due to the mismatch between the model used for design and the actual dynamics.

Figure 12 shows control inputs computed by both architectures to perform MLA and track the references. In both of them, the inner elevators are deflected downwards in order to shift the lift distribution to the inner portion of the wing,

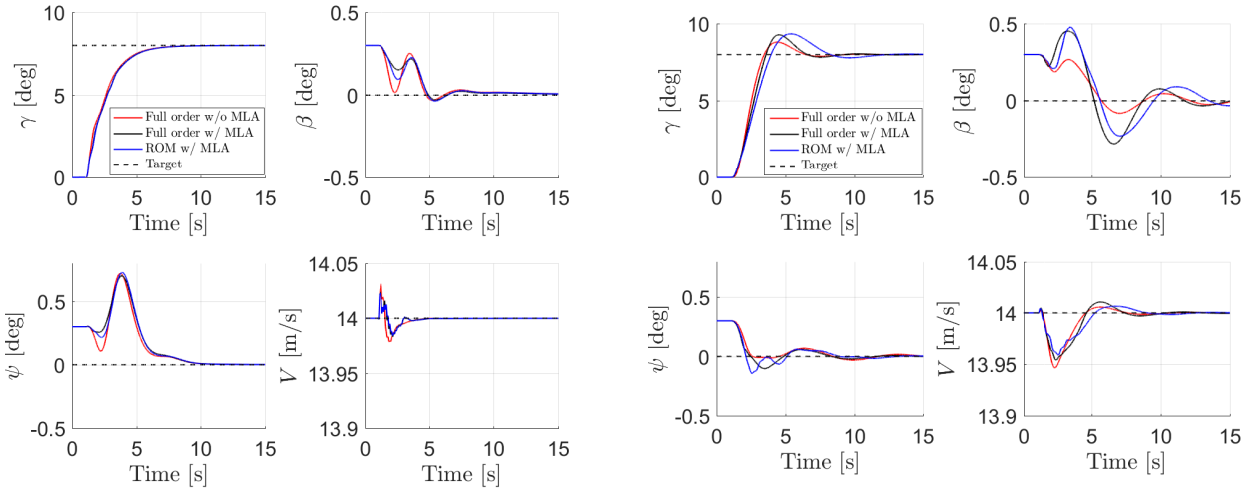

(a) MPC architecture.

(b) RG architecture.

Figure 11 Command tracking performance of the X-HALE very flexible aircraft.

and therefore reduce the root bending moment. In the RG architecture designed with the ROM, the overestimation of the curvature resulted in a larger deflection of the inner elevators to perform MLA. Similar to the case for the flexible aircraft, the outer elevators return to the trim condition after performing the load alleviation in order to reduce drag and the impact on the trajectory of the vehicle.

Incidentally, the impact of the MLA system on the nominal trajectory was small, below 0.4%, as shown in Fig. 13. The impact of the actuation performed by the RG architecture was, in general, greater than the impact in case where the MPC architecture was used.

C. Computational cost

Table 2 shows the maximum and average computation time of the optimizer for each simulation case presented in Sections V.A and V.B, normalized by the sampling time $T_s = 0.02$ s. All simulations were performed on a Dell XPS 15 laptop (Intel i7-7700HQ, 2.8GHZ, 16 MB RAM). The prediction based on the ROM provided a reduction of the average computation time. The level of reduction for the flexible aircraft with the MPC architecture was 5.3%, and 32.0% with the RG architecture. For the very flexible aircraft, the reduction was 8.7% and 55.7%, respectively. In most cases, the maximum computation time was also reduced when the ROM was used for prediction, even though in a smaller scale. However, for the simulation with the ROM and the RG architecture, there was an increase of the maximum computation time due to the violation of constraints. In general, the MPC architecture had lower computational cost. The computational cost was also higher in the very flexible vehicle case.

In most cases, the maximum optimization time of the current implementation of the controllers exceeded the controller sampling time of 0.02 s. Alternative algorithms to solve the quadratic programming problem such as the

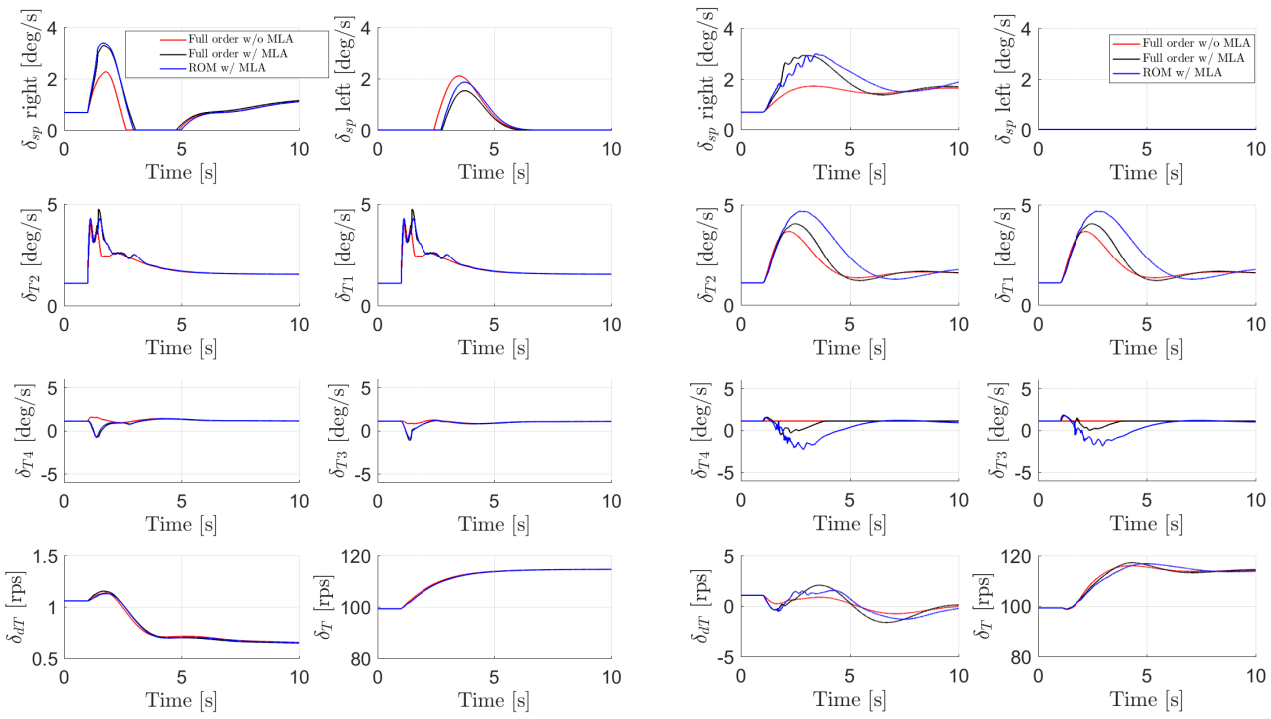

(a) MPC architecture. **(b) RG architecture.**

Figure 12 Time histories of control inputs of X-HALE very flexible aircraft.

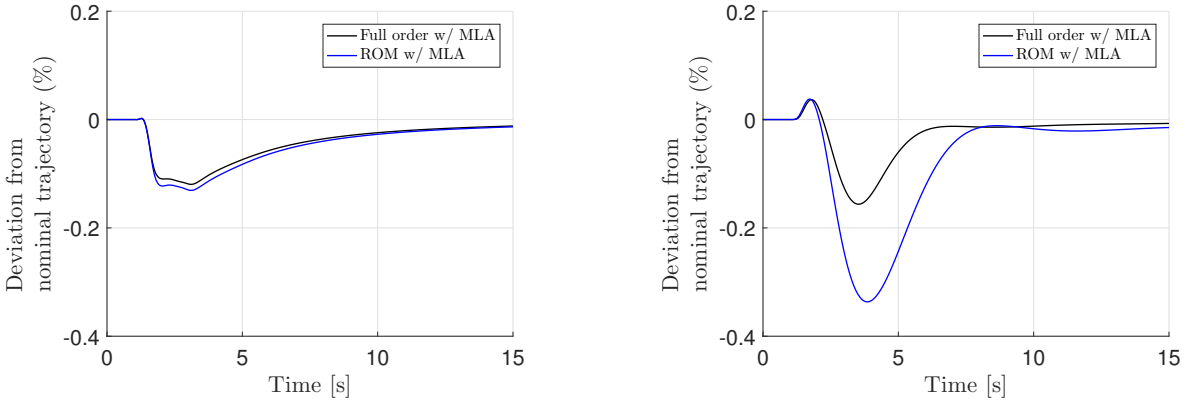

(a) MPC architecture. **(b) RG architecture.**

Figure 13 Trajectory deviation of the X-HALE very flexible aircraft.

regularized and smoothed Fischer-Burmeister method [30] will be considered in future research. In addition, one can also explore the structure, e.g., sparsity, of the matrix in the linearized model, inexact updates, move blocking, and warm-start strategies to reduce the computational footprint of the real-time implementation. Finally, the computational cost of the RG architecture can be lowered by pursuing less flexible designs, such as scalar, vector, command, incremental

Table 2 Maximum and average normalized optimization wall time

	Flexible				Very flexible			
	MPC		RG		MPC		RG	
Model	Max.	Avg.	Max.	Avg.	Max.	Average	Max.	Avg.
Full order w/o MLA	3.24	0.360	3.49	0.365	3.51	0.390	3.63	0.380
Full order w/ MLA	11.7	0.570	79.8	1.67	32.1	1.04	176	3.34
ROM w/ MLA	11.5	0.540	114	1.265	31.3	0.95	176	1.48

or explicit reference governor designs [22].

VI. Conclusion

Two predictive control strategies for MLA applicable to flexible and very flexible aircraft have been introduced: a single MPC controller for output tracking and constraint enforcement, and an LQ-I tracking controller augmented with an MPC in an outer loop that handles constraints. To achieve load alleviation, constraints were imposed on the out-of-plane curvature at the wing root. The controllers were simulated based on nonlinear flexible and very flexible aircraft models. The model for the flexible aircraft was generated by increasing the stiffness of the X-HALE very flexible aircraft model in UM/NAST. A full order linearized model and a reduced-order model were adopted as the prediction models in the MPC design.

Nonlinear simulation results showed that both control strategies were successful in achieving command tracking while enforcing the curvature constraints, resulting in load alleviations around 32-46% for the flexible aircraft, and 42-56% for the very flexible aircraft. However, the tracking performance had to be slowed down on the very flexible aircraft model to avoid high accelerations that cause high structural deflections that are not captured by the linearized models used for prediction.

The use of reduced-order models decreased the average computation time involved in solving MPC optimization problems, with little impact on the controller's performance. Our MPC-based MLA systems, when activated, produced negligible changes in the trajectory of the aircraft, which was the design intent.

Future research opportunities include the application of nonlinear control solutions to the very flexible vehicle to improve the closed-loop response and MLA system performance when the nonlinear structural deformation is significant. Furthermore, the computational cost of MPC solutions need to be lowered in order to facilitate the implementation of the proposed control architectures.

Acknowledgments

The authors would like to thank John Hansen (University of Michigan) for his help in establishing the stiffened X-HALE aircraft model representing a flexible aircraft. The authors also acknowledge Pedro Gonzalez, Zi Yang Pang

and Dominic Liao-McPherson (University of Michigan) for helpful discussions. This material is based upon work supported by Airbus in the frame of the Airbus-Michigan Center for Aero-Servo-Elasticity of Very Flexible Aircraft (CASE-VFA).

References

[1] Cesnik, C. E. S., and Su, W., "Nonlinear Aeroelastic Simulation of X-HALE: a Very Flexible UAV," *49th AIAA Aerospace Sciences Meeting Including the New Horizons Forum and Aerospace Exposition*, Orlando, Florida, USA, 2011, pp. 1–13.

[2] White, R., "Improving the Airplane Efficiency by Use of Wing Maneuver Load Alleviation," *Journal of Aircraft*, Vol. 8, No. 10, 1971, pp. 769–775.

[3] Cesnik, C. E. S., Senatore, P. J., Su, W., Atkins, E. M., and Shearer, C. M., "X-HALE: A Very Flexible Unmanned Aerial Vehicle for Nonlinear Aeroelastic Tests," *AIAA Journal*, Vol. 50, No. 12, 2012, pp. 2820–2833.

[4] Cesnik, C. E. S., Palacios, R., and Reichenbach, E. Y., "Reexamined Structural Design Procedures for Very Flexible Aircraft," *Journal of Aircraft*, Vol. 51, No. 5, 2014, pp. 1580–1591.

[5] Simpson, R. J., Palacios, R., Hesse, H., and Goulart, P., "Predictive Control for Alleviation of Gust Loads on Very Flexible Aircraft," *55th AIAA/ASME/ASCE/AHS/SC Structures, Structural Dynamics, and Materials Conference*, National Harbor, Maryland, USA, 2014, pp. 1–25.

[6] Nguyen, N., and Hashemi, K., "Performance Optimizing Adaptive Control with Time-Varying Reference Model Modification," *18th Eighteenth Yale Workshop on Adaptive and Learning Systems*, New Haven, Connecticut, USA, 2017, pp. 1–6.

[7] Li, H., Zhao, Y., and Hu, H., "Adaptive Maneuver Load Alleviation via Recurrent Neural Networks," *Journal of Guidance, Control, and Dynamics*, Vol. 40, No. 7, 2017, pp. 1821–1828.

[8] Lavretsky, E. Y., and Henderson, D. K., "A Neural Network-Based Approach to Active Structural Mode Suppression for Flexible Transport Aircraft," *Proceedings of American Control Conference*, San Diego, California, USA, 1999, pp. 4168–4172.

[9] Maraniello, S., Simpson, R. J., and Palacios, R., "Optimal Manoeuvres with Very Flexible Wings," *Proceedings of 57th AIAA/ASCE/AHS/ASC Structures, Structural Dynamics, and Materials Conference*, Reston, Virginia, 2016, pp. 1–17.

[10] Gaulocher, S. L., Roos, C., and Cumer, C., "Aircraft Load Alleviation During Maneuvers Using Optimal Control Surface Combinations," *Journal of Guidance, Control, and Dynamics*, Vol. 30, No. 2, 2007, pp. 591–600.

[11] Chiu, S., Chand, S., Moore, D., and Chaudhary, A., "Fuzzy Logic for Control of Roll and Moment for a Flexible Wing Aircraft," *IEEE Control Systems*, Vol. 11, No. 4, 1990, pp. 42 – 48.

[12] Dillsaver, M. J., Kalabić, U. V., Kolmanovsky, I. V., and Cesnik, C. E. S., "Constrained Control of Very Flexible Aircraft Using Reference and Extended Command Governors," *American Control Conference (ACC), 2013*, IEEE, Washington, District of Columbia, USA, 2013, pp. 1608–1613.

[13] Kopf, M., Giesseler, H. G., Varutti, P., Faulwasser, T., and Findeisen, R., "On the Effect of Enforcing Stability in Model Predictive Control for Gust Load Alleviation," Chicago, Illinois, USA, 2015, pp. 2329–2334.

[14] Kopf, M., Bullinger, E., Giesseler, H. G., Adden, S., and Findeisen, R., "Model Predictive Control for Aircraft Load Alleviation: Opportunities and Challenges," *2018 Annual American Control Conference (ACC)*, IFAC, Milwaukee, Wisconsin, USA, 2018, pp. 2417–2424.

[15] Giesseler, H. G., Kopf, M., Varutti, P., Faulwasser, T., and Findeisen, R., "Model Predictive Control for Gust Load Alleviation," *4th IFAC Conference on Nonlinear Model Predictive Control*, Vol. 4, IFAC, Noordwijkerhout, Netherlands, 2012, pp. 27–32.

[16] Liu, X., and Sun, Q., "Improved LQG Method for Active Gust Load Alleviation," *Journal of Aerospace Engineering*, Vol. 30, No. 4, 2017, pp. 1 –13.

[17] Fabre, P., Tron, X. L., and Lacoste, P., "System for Reducing the Forces Applied to Wings and Particularly to the Root of the Wings of an Aircraft in Flight," *United States Patent 5186416*, 1993.

[18] Burlion, L., Poussot-Vassal, C., Vuillemin, P., Leitner, M., and Kier, T., "Longitudinal Manoeuvre Load Control of a Flexible Large-Scale Aircraft," *Proceedings of the 19th World Congress - The International Federation of Automatic Control (IFAC)*, Vol. 19, IFAC, Cape Town, South Africa, 2014, pp. 3413–3418.

[19] Cook, R. G., Palacios, R., and Goulart, P., "Robust Gust Alleviation and Stabilization of Very Flexible Aircraft," *AIAA Journal*, Vol. 51, No. 2, 2013, pp. 330–340.

[20] Yang, Y., Wu, Z., and Yang, C., "Control Surface Efficiency Analysis and Utilization of an Elastic Airplane for Maneuver Loads Alleviation," *54th AIAA/ASME/ASCE/AHS/ASC Structures, Structural Dynamics, and Materials Conference*, Boston, Massachusetts, USA, 2013, pp. 1–7.

[21] Andrews, S. P., "Modelling and Simulation of Flexible Aircraft: Handling Qualities with Active Load Control," Ph.D. thesis, Cranfield University, Cranfield, UK, 2011.

[22] Garone, E., Cairano, S. D., and Kolmanovsky, I., "Reference and Command Governors for Systems with Constraints: A Survey on Theory and Applications," *Automatica*, Vol. 75, 2017, pp. 306–328.

[23] Kalabić, U. V., Kolmanovsky, I., and Gilbert, E. G., "Reduced Order Extended Command Governor," *Automatica*, Vol. 50, No. 5, 2014, pp. 1466–1472.

[24] Gilbert, E. G., and Ong, C. J., "Constrained Linear Systems with Hard Constraints and Disturbances: An Extended Command Governor with Large Domain of Attraction," *Automatica*, Vol. 40, 2011, pp. 334–340.

[25] Su, W., and Cesnik, C. E. S., "Strain-based Geometrically Nonlinear Beam Formulation for Modeling Very Flexible Aircraft," *International Journal of Solids and Structures*, Vol. 48, 2011, pp. 2349 – 2360.

[26] Pang, Z. Y., "Modeling, Simulation and Control of Very Flexible Unmanned Aerial Vehicle," Ph.D. thesis, University of Michigan, Ann Arbor, MI, USA, 2018.

[27] Muller, P. C., and Weber, H. I., "Analysis and Optimization of Certain Qualities of Controllability and Observability for Linear Dynamical Systems," *Automatica*, Vol. 8, 1972, pp. 237–246.

[28] Mackenroth, U., *Robust Control Systems: Theory and Case Studies*, Springer Science & Business Media, 2004.

[29] Ferreau, H., Kirches, C., Potschka, A., Bock, H., and Diehl, M., "qpOASES: A Parametric Active-set Algorithm for Quadratic Programming," *Mathematical Programming Computation*, Vol. 6, No. 4, 2014, pp. 327–363.

[30] Liao-McPherson, D., Huang, M., and Kolmanovsky, I., "A Regularized and Smoothed Fischer-Burmeister Method for Quadratic Programming with Applications to Model Predictive Control," *IEEE Transactions on Automatic Control*, 2018.